Investigation of the right first-time distortion compensation approach in laser powder bed fusion of a thin manifold structure made of Inconel 718

Shukri Afazov, Hafizur Rahman, Ahmad Serjouei

Department of Engineering, School of Science and Technology, Nottingham Trent University, Nottingham, UK

Abstract

The research work first demonstrates modelling techniques for distortion prediction of laser powder bed fusion (LPBF) using the inherent strain approach implemented in structural finite element analyses. The prediction of distortion is compared with experimentally measured results of a thin manifold structure made of Inconel 718. The predicted distortions were used to verify the right first-time approach for distortion compensation where the thin manifold structure was first simulated. The distortion was then compensated using mapping techniques across different source meshes, and the component was finally manufactured using LPBF. Two components were built, one with compensation and one without compensation. The results showed that the right first-time approach compensated the distortion for the majority of the part. There were areas where the compensation was not accurate due to overpredictions of the distortion.

Keywords: distortion prediction, distortion compensation, finite element method, inherent strain method

1. Introduction

Additive manufacturing (AM) has attracted significant interest within the last three decades in addressing the need for time- and cost-effective production in industry [1]. While AM provides unparalleled features such as design flexibility, removal of material waste, etc., it suffers from some features like large surface roughness, internal defects, and residual stress. Inconsistent shrinkage [2] and nonhomogeneous thermal gradients and rapid localized cooling which lead to residual stress [3] are the causes of part distortion. Residual stresses can be generated when the material exhibits phase transformations [4]. For example, effect of phase transformation strain on residual stress of different materials printed using the LPBF technology has been extensively studied [5–8]. Researchers studied the dependence of the residual stresses in LPBF on the process parameters such as beam intensity, beam scan velocity, scanning strategy, process conditions like layer thickness, part size, as well as material and powder properties [9–11], part geometry [12] and heat transfer [13]. Bartlett and Li [11] classified the main process parameters affecting the residual stress formation and distortion in LPBF technologies to three main categories: (1) beam parameters such as power, volumetric energy input and scan speed; (2) process condition and geometry considerations such as layer thickness, part geometry and build plate temperature; (3) scan strategy parameters such as raster pattern, interlayer dwell time and scanning strategy.

Lack of dimensional accuracy due to presence of residual stresses and distortion is specifically one of the challenges in LPBF. Hence, the mitigation of residual stresses and distortion in LPBF has been the focus of research in recent years. Simulation of parts during and after printing is an effective way to mitigate parts failure due to distortion [14]. Peter et al. [15] from Electro Optical Systems (EOS) company compared the capabilities of five different simulation software tools, namely ANSYS Additive Print, Autodesk, MSC, Additive Works, and Atlas3D, for the sake of providing strengths and weaknesses of these software, specially to simulate

distortion in a wide range of test artifacts which were printed by LPBF using compensated parts suggested by the software tools. The use of dynamic mesh has proven reducing the model size and computational cost in thermal finite element modelling of LPBF technologies using the 3DSIM tool [16]. Beside 3DSIM, AM simulation tool Pan Computing [17] and finite element code Deal.II [18] have used a dynamic mesh for simulation of AM. Machine learning has also been used for AM simulation [19,20]. Francis and Bian [21] used deep learning approach for distortion mitigation of laser based AM. Pal et al. [22,23] developed a thermomechanical finite element frameworks to predict the anisotropic behaviour, residual stress and distortion in parts in a time-efficient manner. Mukherjee et al. [24] studied, through a coupled thermal fluid flow and mechanical model, the effects of laser-based AM process variables on the residual stresses and distortion. They showed that combined effect of increase of the scanning velocity and decrease of the laser density results in lower thermal strains, hence lower residual stresses. Mukherjee et al. [25] showed that distortion in laser-assisted AM reduces by decreasing the layer height and the laser intensity. Williams et al. [26] simulated the temperature and residual stresses in LPBF using thermo-mechanical numerical analysis. They showed a prediction of distortion for 316L stainless steel bridge and Inconel 718 cuboidal parts with 5% and 10% accuracy, respectively. Denlinger et al. [27] used a three-dimensional (3D) thermo-elasto-plastic analysis to predict residual stress and distortion of a wire-fed electron beam deposited Ti-6Al-4V part. They demonstrated a stress relaxation incorporated in the model. Biegler et al. [28] developed a transient thermo-mechanical model for mitigation of distortion of industrial parts built using directed energy deposition (DED). They showed a reduction of over 65% distortion for a 316L stainless steel thin-walled turbine blade using numerical simulation after the geometry has been modified by changing the nodal coordinates of the mesh using predicted displacements. For large in size geometries, the thermo-mechanical modelling techniques with the use of a heat source is computationally expensive. This has pushed the development of fast predictive models. For example, analytical thermal model combined with lumping of layers and calibration has been proposed and validated to overcome the computational challenges [29]. Another fast predictive approach is the use of an inherent strain. Murakawa et al. [30] were among the pioneers who utilised the inherent strain method for prediction of deformation and residual stress in welding using a thermal-elastic-plastic finite element analysis. Huang et al. [31] used an inherent strain based time-scaling technique in their fast predictive explicit thermomechanical finite element model of wire and arc additive manufacturing (WAAM). They envisaged that the method can be used to develop digital twin of WAAM with the purpose of reducing the time and cost of analysis. Chen et al. [32] proposed a multiscale method in which inherent strains are employed to pre-scale part distortion in Direct Metal Laser Sintering (DMLS). They showed that by using their proposed method, the computational time has substantially reduced. The inherent strain approach has shown accurate predictions of distortion of Inconel 718 components, e.g. an aero-casing [33] and impeller [34] where the inherent strains have been directly prescribed without the use of finite element thermal transient analysis.

The distortion compensation can be achieved by pre-distorting the geometry using the predicted distortion from the numerical method. The right first-time approach based on numerical perdition was demonstrated on a turbine blade [29]. Yaghi et al. [35] implemented a similar analogy of pre-distorting the geometry to compensate for distortion developed due to the combined effects of AM building process as well as post machining. They mitigated the distortion of a stainless-steel impeller manufactured by LPBF. An alternative approach is to use measured data using optics to calculate the distortion and change the geometry [36,37]. This approach requires a physical build to measure the distortion, while the predictive models can be used to pre-distort the geometry without the need of making a physical build. The main

challenge in the physics-based predictive models is the accuracy of the prediction, which might be particularly challenging for thin structures [38].

Despite the conducted research in distortion prediction and compensation in LPBF, the right first-time distortion compensation of thin structures using predictive models has not been researched. The current paper builds on the inherent strain approach for prediction of distortion that has been validated for Inconel 718 industrial components processed by LPBF, i.e. an aero-casting [33] and an impeller [34]. The inherent strain approach is applied to a thin Inconel 718 manifold structure processed by LPBF in this study. The inherent strain approach was implemented into two non-linear commercial finite element codes, namely ABAQUS and ANSYS Mechanical. The main motivation of using two commercial finite element codes was to benchmark the results with the developed modelling so that greater confidence is obtained before the predicted results are used for distortion compensation. The predicted distortion has been used to pre-distort the geometry and compensate distortion. The compensated thin manifold structure was compared with the data-driven distortion compensation approach presented in [37].

The novelty of the current paper is the comparison of distortion compensation, using different material models, from numerical solutions versus data-driven distortion compensation approach using optically scanned data of a build.

2. Experimental set-up

A thin manifold structure was designed with a height of 210 mm and a thickness of 1.5 mm. The CAD model was used to create custom generated solid support structure connecting the part to the build plate. The solid support structures were designed to conduct more heat to the build plate and reduce the impact of the thermal effects (e.g. potential microstructural changes due to phase transformation). An EOS M290 (EOS, Krailling, Germany) LPBF AM machine was used to manufacture the part under an Argon atmosphere, a laser power of 190W, a laser scanning velocity of 800 mm/s, a layer thickness of 40 μm, a hatching distance of 90 μm and a stripe scanning strategy. Preheating temperature of 100 °C to the build plate, and a 10 s dwell time between two successive deposited layers were applied. There was no post heat treatment applied to the build plate. The process parameters have been fixed in this study assuming that distortion compensation is applied in production process. The manifold was printed out of Inconel 718 powder from LPW Technology Inc. (LPW, Runcorn, UK) with average particle size between 15-45 μm. Virgin gas-atomized powder, from a sealed moisture-proof container, was used for printing. Bulk density and tap density of the powder were 4.25 g/cm^3 and 4.81 g/cm^3, respectively. A printed part after compensation and a block sample are shown in Figure 1. After the build completion, the part was optically scanned on the build plate using a blue light technology embedded in the GOM ATOS Triple Scan optical measurement system equipped with two 12-megapixel resolution cameras capable of achieving an accuracy of 10 microns. Prior to the scanning of the manifold, the block sample was scanned to calibrate the blue scanner. The scanned data representing a cloud of points was converted into a surface mesh and used to calculate the surface deviations.

Figure 1: LPBF built of a thin Inconel 718 manifold structure

3. Distortion prediction and compensation models

Two commercial software solvers (ANSYS Mechanical and ABAQUS) were used to model the LPBF build process. The motivation of using these two solvers is that they have been widely used in the simulation of thermo-mechanical non-linear manufacturing process such as welding. To simulate part-scale component, the inherent strain approach was implemented to simulate the build process. Afazov et al. [33] and O'Brien at al. [34] used the inherent strain methods implemented in ABAQUS to predict the distortion of industrial components made of Inconel 718. Motivated by the accuracy of the predicted distortions for Inconel 718 processed by LPBF, the same inherent strain approach was implemented in ABAQUS and ANSYS Mechanical for the thin manifold structure to understand how sensitive the method is by using different finite element codes. It should be noted that the inherent strain approach does not consider the thermal history.

3.1 Finite element models in ANSYS Mechanical

The geometry of the thin manifold structure was imported into ANSYS Mechanical. The geometry was sliced with 1 mm layers and then meshed with 142,319 ten-node quadratic tetrahedral elements (see Figure 2). The mesh generated with quadratic tetrahedral elements better represents the geometrical features in comparison to the use of voxel based elements where the mesh size is more critical. Considering that the actual layer thickness is 40 µm, this means that 25 layers are lumped together in the model. The rationale behind this assumption was to reduce computational time. Also, the same layer thickness was assumed for industrial components of Inconel 718 and the predicted distortions were in very good corelation with the experimental results [33, 34]. The build plate and the support structures were modelled by applying zero displacements in all direction to the bottom surface of the part. This assumption is representative considering the high stiffness of the build plate and high bending and tensile stiffness of the support structures due to their solid nature and low height (see Figure 1).

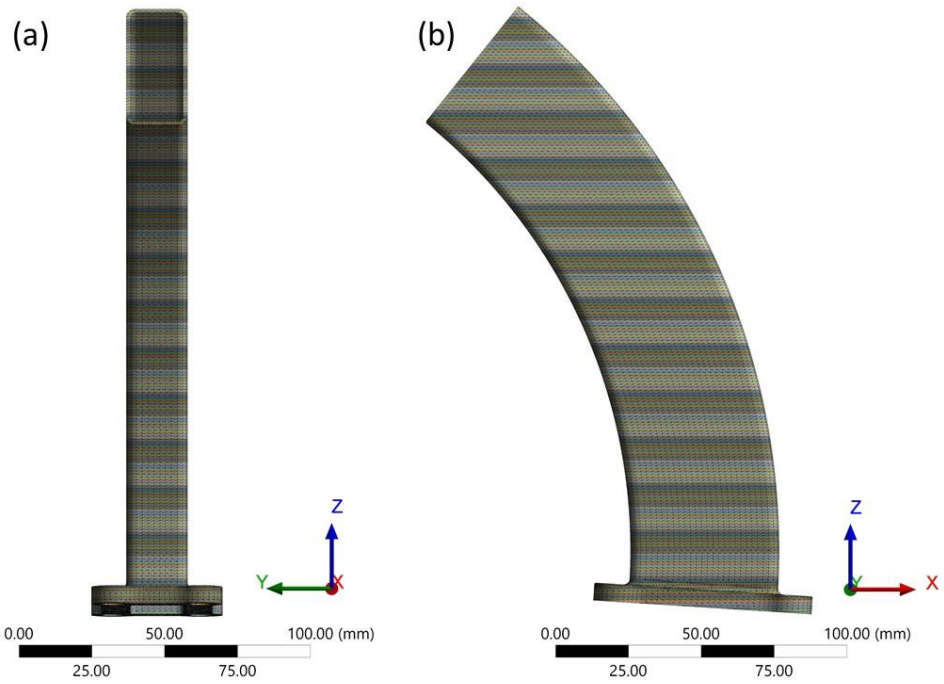

Figure 2: Sliced and meshed geometry in ANSYS Mechanical: (a) front view (b) side view

Elements for each of the layers were activated using the "element birth" technique. The "element birth" technique is based on the Lagrangian finite element formulations that are capable of activation and deactivation of elements. The technique has been implemented into commercial software solvers and used to model metal deposition, welding and metal powder bed fusion [39-43]. When the elements were activated, a strain was applied to them. The strain was applied by changing the temperature from zero to a value of one and assigning the strain value as a property of the coefficient of thermal expansion.

The element birth technique in ANSYS works based on the principle that all elements are assigned to the stiffness matrix at the start of the analysis. The "death" elements are represented by "dummy properties" or properties with a stiffness close to zero. The "birth" element technique changes the martial properties for the activated elements. The challenge with simulation of the build process is that all activated elements in the model induce deformations due to the induced residual stresses. The elements which are not activated do follow the deformation of the model because they exist in the stiffness matrix. This means that when they are activated to represent a deposited layer, they will be displaced due to the fact that they are part of the stiffness matrix and displacements are calculated at the nodal points of those elements. To mitigate this problem, a boundary condition with zero displacement in the x, y and z directions is applied to all nodes belonging to the non-active or "death" elements. This was done by APDL commands in the ANSYS Mechanical environment where all nodes above the deposited layer were given zero displacements in all degrees of freedom.

As mentioned above, Afazov et al. [33] and O'Brien at al. [34] demonstrated excellent prediction of distortion using the inherent strain approach. They used elastic-perfectly-plastic isotropic material model. It is well known that the yield strength in the build direction is lower compared to the two-transverse directions. The same is valid for the material stiffness which also shows orthotropic behaviour. To understand how sensitive the distortion prediction is, two material models were investigated in this study (isotropic and anisotropic). The isotropic

material model with perfect elastic-plastic material model was applied. The applied strain values in all directions was determined by the ratio of the yield stress of 620 MPa over the modulus of elasticity of 170 GPa [33,34]. This resulted compressive strain of -0.0037 was applied to the activated elements by applying a coefficient of thermal expansion of -0.0037 and changing the temperature from zero to a value of one in the model. The rational of applying a compressive strain is to shrink the finite elements to a level where the material yields, and calculations based on the plasticity theory are conducted to calculate the tensor strains and stresses. This approach is deferent from the conventional inherent strain approach which relies on the application of the Hooke's law to calculate the tensor stressors based on the applied inherent strain in each direction and the prescribed Young's modulus.

The second material model implemented in ANSYS Mechanical consist of an orthotropic elastic model combined with an anisotropic model with perfect plasticity using Hill's yield criterion [44]. The orthotropic elastic material properties are obtained from the data for Inconel 718 provided by EOS [45]. The Young's modulus, the Poisson's ratio and the shear modules of the orthotropic elastic material model are given in Table 1. The equivalent (effective) stress in the Hill's yield criterion is given by:

$$\hat{\sigma} = \sqrt{F(\sigma_{22} - \sigma_{33})^2 + G(\sigma_{33} - \sigma_{11})^2 + H(\sigma_{11} - \sigma_{22})^2 + 2L\sigma_{23}^2 + 2M\sigma_{13}^2 + 2N\sigma_{12}^2} \quad (1)$$

where $\hat{\sigma}$ is the equivalent (effective stress); σ_{11}, σ_{22}, σ_{33}, σ_{23}, σ_{13}, σ_{12} are the stress tensors; and F, G, H, L, M and N are coefficients given by:

$$F = \frac{1}{2}\left(\frac{1}{R_{22}^2} + \frac{1}{R_{33}^2} - \frac{1}{R_{11}^2}\right) \quad (2)$$

$$G = \frac{1}{2}\left(\frac{1}{R_{33}^2} + \frac{1}{R_{11}^2} - \frac{1}{R_{22}^2}\right) \quad (3)$$

$$H = \frac{1}{2}\left(\frac{1}{R_{11}^2} + \frac{1}{R_{22}^2} - \frac{1}{R_{33}^2}\right) \quad (4)$$

$$L = \frac{3}{2}\left(\frac{1}{R_{23}^2}\right) \quad (5)$$

$$M = \frac{3}{2}\left(\frac{1}{R_{13}^2}\right) \quad (6)$$

$$N = \frac{3}{2}\left(\frac{1}{R_{12}^2}\right) \quad (7)$$

The directional yield ratios (R_{11}, R_{22}, R_{33}, R_{12}, R_{13} and R_{23}) describe the directional dependencies. They are obtained based on the anisotropic data for Inconel 718 provided by EOS [45], and the directional yield ratios are given in Tables 2 where an isotropic yield stress of 620 MPa was used [45]. All anisotropic material properties are applied at room temperature because the inherent strain approach is not dependent on temperature. The motivation behind the anisotropic model is to compare the results with the isotropic material model and understand the impact of the anisotropic effect on the distortion prediction using the inherent strain method.

Table 1: Anisotropic elastic properties at room temperature based on the data from EOS [45]

Young's Modulus	Young's Modulus	Young's Modulus	Poison ratio in	Poison ratio in	Poison ratio in	Shear Modulus	Shear Modulus	Shear Modulus

(E_x), GPa	(E_y), GPa	(E_z), GPa	the xy plane	the yz plane	the xz plane	(Gxy). GPa	Gyz). GPa	Gxx). GPa
170	170	150	0.3	0.3	0.3	65	57	57

Table 2: Constants for Hill's yield criterion obtained based on the data from EOS [45]

Yield Stress, MPa	R_{11}	R_{22}	R_{33}	R_{12}	R_{23}	R_{13}
620	1.2	1.2	1	0.9	0.9	0.9

3.2 Finite element model in ABAQUS

A finite element model using the same mesh generated in ANSYS and boundary conditions at the bottom surface was developed in ABAQUS. The same isotropic material model with yield stress of 620 MPa and Young's Modulus of 170 GPa was used. The same isotropic compressive strain of -0.0037 was applied for each activated layer using the UEXPAN user-defined subroutine which enables to prescribe the incremental strain value directly into the solver [34]. This is the same approach as the change of temperature from 0 to 1 and prescribing the inherent strain value by the coefficient of thermal expansion. The "birth" and "death" element activation techniques of ABAQUS were utilised. In comparison to ANSYS Mechanical, ABAQUS reconstructs the stiffness matrix after the elements are activated with the "birth" technique. This technique activates the elements at the modelled layers. Therefore, no additional boundary condition was required in this model. As mentioned above, the main aim of developing a model in ABAQUS is to benchmark the results and understand the sensitivity in distortion prediction using different finite element codes as well as element activation techniques and the use of different material models.

3.3 Distortion compensation using mapping

The right first-time distortion compensation approach relies on changing the geometry of the initially designed thin manifold in the opposite direction without the need of a build, and fully relying on accurate prediction of distortion. For the distortion compensation, a refined surface mesh is required in order to capture all predicted local deformations. Therefore, a refined surface mesh with triangles that have a maximum edge size of 1 mm was generated. The predicted displacements in the x, y and z directions from the finite element model are mapped into the refined surface mesh using the element shape function mapping techniques embedded in the open source code FEDES [46]. The coordinates in the x, y and z directions are changed in the refined surface mesh by subtracting the mapped displacements. For example, if the coordinates of a node in the x, y and z directions were [100, 200, 250] and the mapped displacements from the simulation for that node were [0.2, -0.4, 0.6], the compensated coordinates are [100-0.2, 200 - (-0.4), 250-0.6] or [99.8, 200.4, 149.4]. The same approach is applied to all nodes of the refined surface mesh.

4. Results and discussion

The predicted displacements at the end of the build are shown in Figures 3-5 in the x, y, and z directions for the three finite element models. It can be seen that the predicted patterns are very similar. The maximum predicted displacements are given in Table 3 where the two isotropic models implemented in ABAQUS and ANSYS Mechanical predicted identical maximum displacements in the x and z directions, while the difference in the y direction was less than

3%. This indicated that the two different element activation techniques in ABAQUS and ANSYS Mechanical did not affect the predicted distortion, hence both techniques can be used for the right first-time distortion compensation. The anisotropic material model showed differences of approximately 5%. As the difference was not significant between the isotropic and anisotropic material models, the results from the isotropic model were used to compensate the geometry before printing. The predicted displacements from the ANSYS and ABAQUS isotropic models were very close. However, the ANSYS results were used for the compensation of the geometry. As the intention was to understand the right first-time distortion compensation approach in this study, no validation step was used for the thin manifold structure.

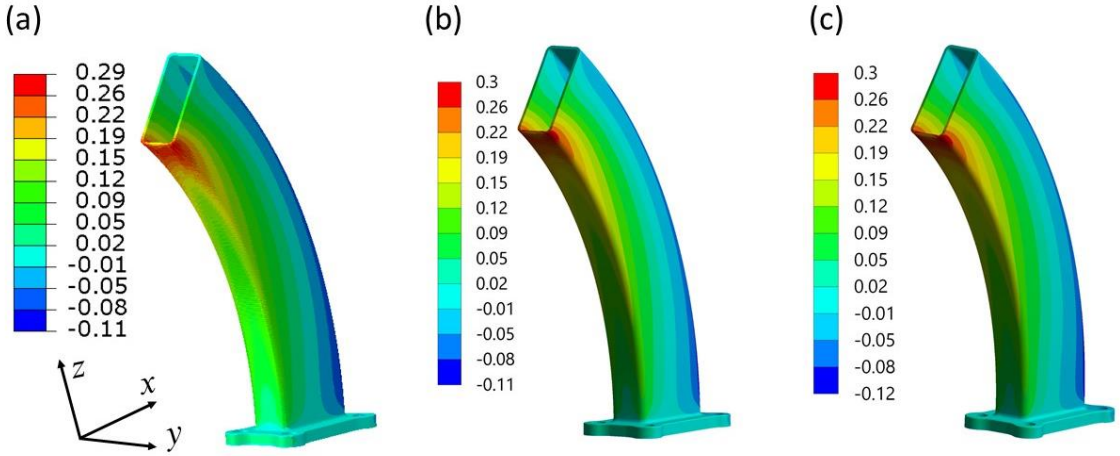

Figure 3: Comparison of predicted displacements in the x direction: (a) ABAQUS with isotropic material model; (b) ANSYS with isotropic material model; and (c) ANSYS with anisotropic material model. Units are in mm.

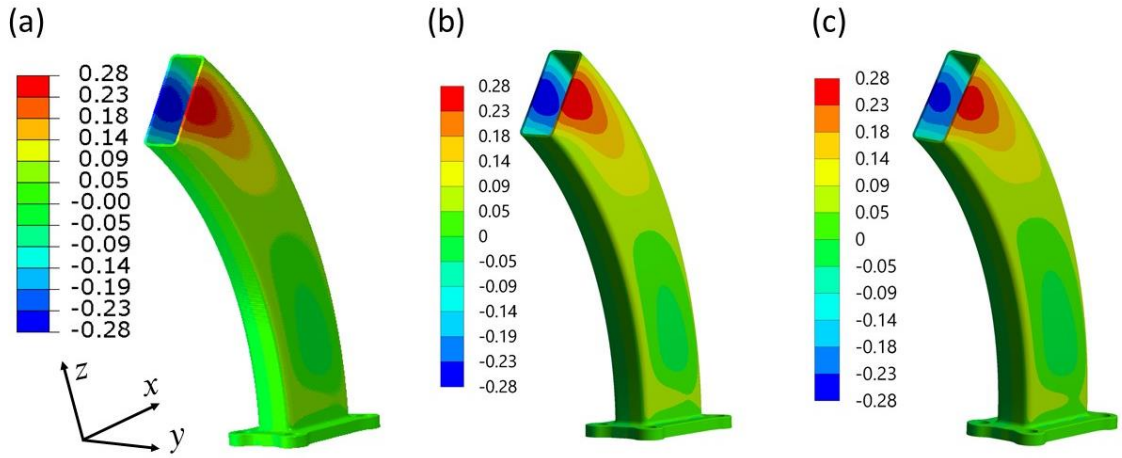

Figure 4: Comparison of predicted displacements in the y direction: (a) ABAQUS with isotropic material model; (b) ANSYS with isotropic material model; and (c) ANSYS with anisotropic material model. Units are in mm.

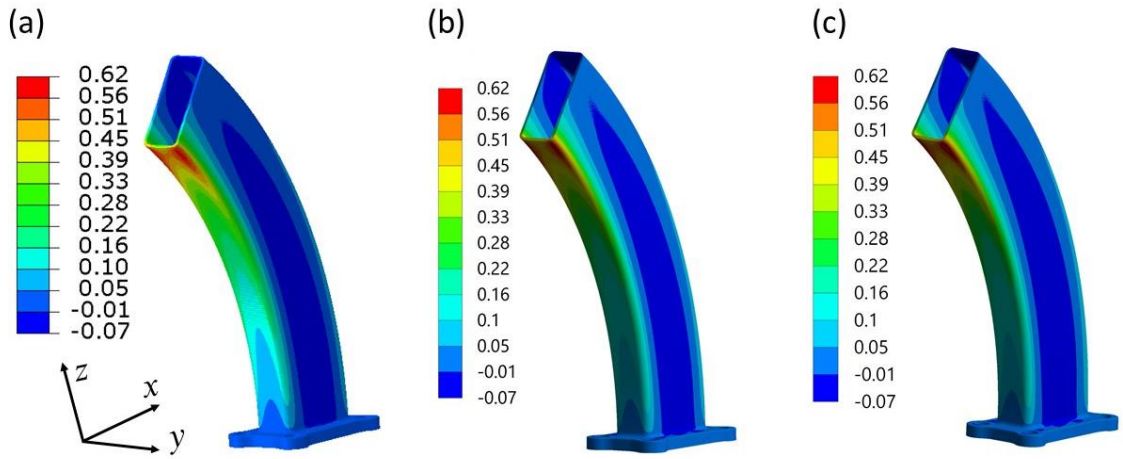

Figure 5: Comparison of predicted displacements in the z (build) direction: (a) ABAQUS with isotropic material model; (b) ANSYS with isotropic material model; and (c) ANSYS with anisotropic material model. Units are in mm.

Table 3: Comparison of predicted maximum displacements

Max. displacement	ABAQUS isotropic	ANSYS isotropic	ANSYS anisotropic
x direction	0.28	0.28	0.26
y direction	0.29	0.30	0.30
z direction	0.62	0.62	0.64

Figure 6 compares the surface deviations for the thin manifold structure with the predicted shape and the compensated one. It can be seen that the compensated deviations are in the opposite direction indicating that the mapping step was correctly applied. The compensated thin manifold structure (Figure 6b), as well as the original design were printed in order to understand how accurate the predictions were. The data-driven compensation approach applied to the same thin manifold structure by Afazov et al. [37] was used to compare the accuracy of distortion compensation using the right first-time approach. Figures 7a, 7b and 7c show the distortion deviations for the as-build thin manifold without any compensation applied, the compensated geometry using the isotropic material model with the inherent strain method in ANSYS Mechanical, and the data-driven distortion compensation results presented in [37], respectively. It can be seen that the right first-time approach managed to compensate the distortion for most of manifold. However, the overall compensated distortion was above +0.25mm. Comparing the predicted deviations (Figure 6a) to the measured deviations (Figure 7a), it can be seen that the model has overpredicted the distortion at the top part of the inner surface which is the reason for the inaccurate compensation in that area. For the areas where the predictions were accurate, the compensation worked too.

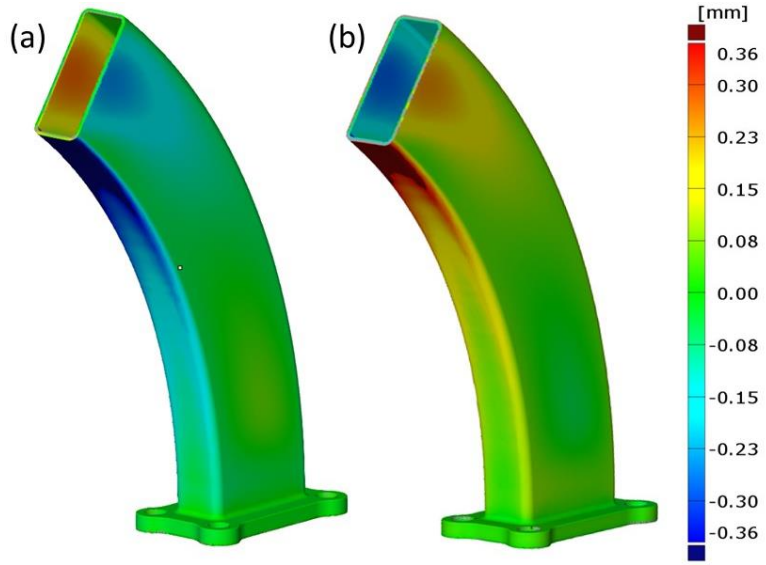

Figure 6: Comparison of distortion deviations: (a) Predicted distorted geometry; (b) Compensated geometry after mapping of displacements. Units are in mm.

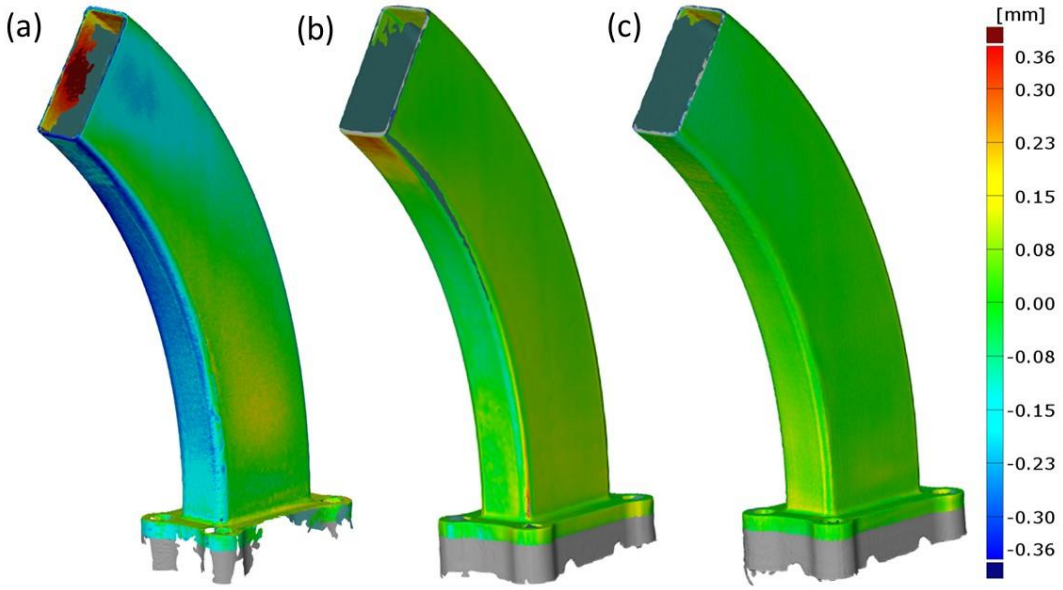

Figure 7: Distortion deviations: (a) as-build without any compensation; (b) after compensation using predicted distortion – right first-time approach; (c) data-driven approach using optically scanned data [37]. Units are in mm. Note that the grey area represents scanned data where distortion deviations from the scanned data to the original CAD geometry are not calculated.

The results from Figures 7b and 7c were further analysed by presenting more views and data points. Figures 8 and 9 show four additional views of the distortion deviations for the right-first time and the data-driven distortion compensation approaches, respectively. For each of the presented sides, seven data points were generated at the middle of each face. Analysing the results for the right-first time approach from Figure 8, the distortion deviations is in the range of -0.02mm – +0.17mm for the front, rear and the outer side views. The distortion deviations for the inner side view was in the range of -0.09mm – +0.26mm. In comparison, the distortion deviations for the data-driven approach from Figure 9 were in the range of -0.08mm – +0.11mm

for all views. Also, the data-drive approached showed better distribution of the compensated distortion across the entire manifold geometry.

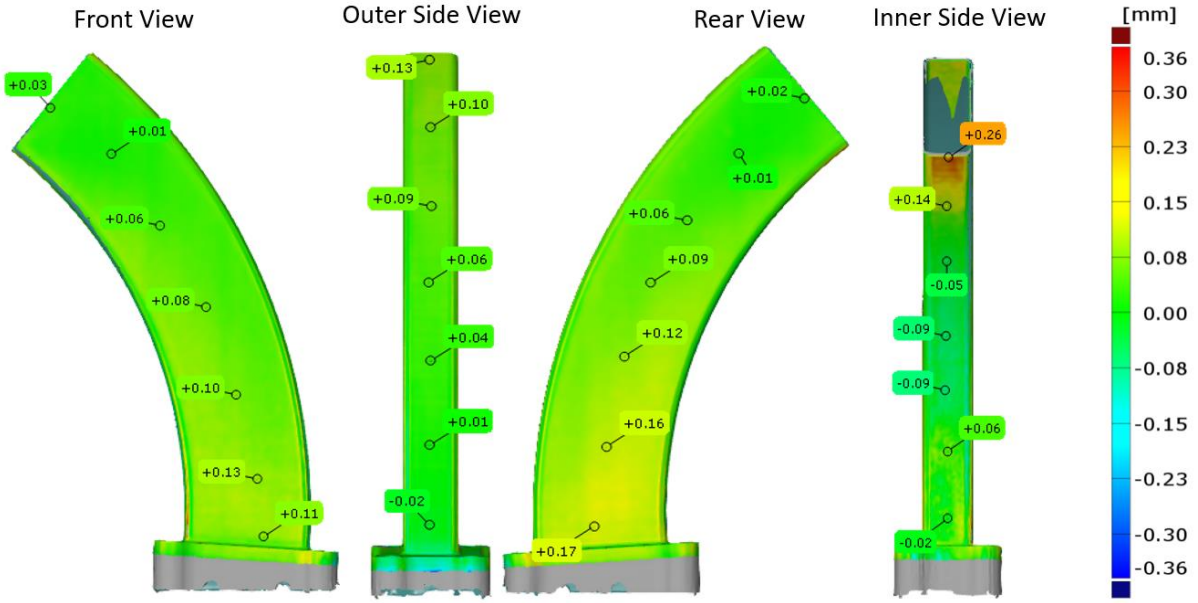

Figure 8: Distortion deviation: results from the compensation using predicted distortion – right first-time approach. Units are in mm.

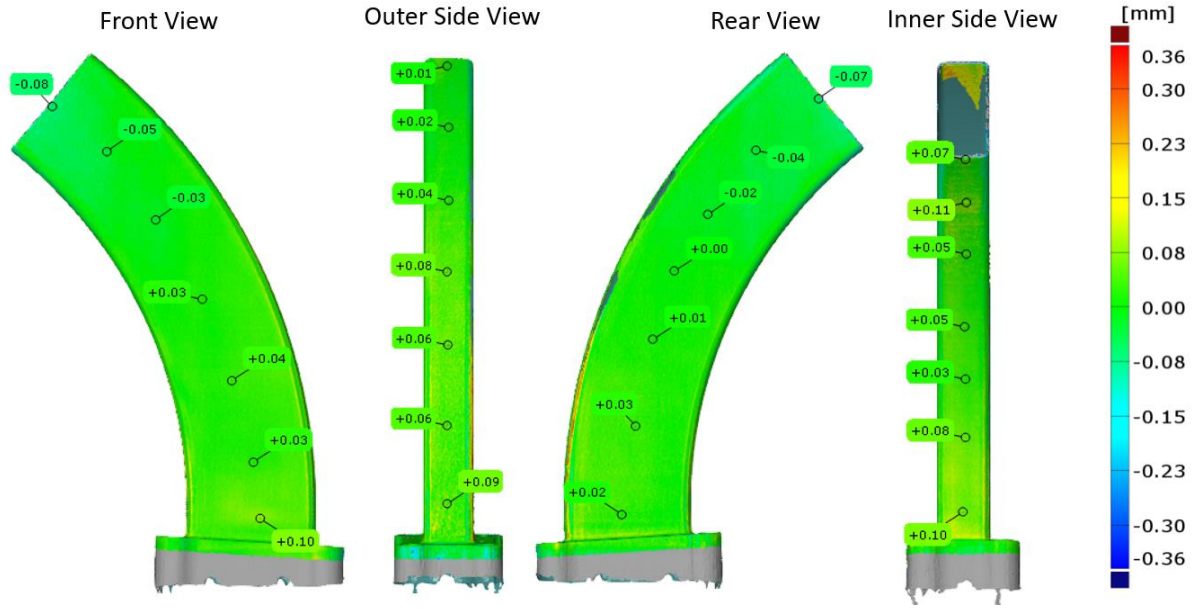

Figure 9: Distortion deviation: results from the data-driven compensation using optically scanned data [37]. Units are in mm.

Despite that the predictive models managed to capture most of the distortion, the presented thin manifold structure appeared to be a challenging geometry for the prediction of distortion using the inherent strain method. In contrast, the data-driven approach has shown better results as it used measured data. However, the data-driven approach requires a physical build. Also, measurements of internal features which are not accessible by optical systems would not generate data. This requires mathematical interpolations which could be associated with errors. This study showed that the right first-time approach has the potential to compensate distortion, but some limitations in the accuracy still exist in the predictive models of distortion of thin

structures which are subjected to buckling deformation. Therefore, further research would be needed to understand the limitations with the distortion predictive modelling techniques on a wide range of geometries. For instance, investigation of the change of thickness of different in size and shape hollow structures would be an important step forward to understand the real geometrical limitations of the predictive models. Knowing the geometrical limitations, a better decision could be formed which components and geometrical features can be compensated for distortion using the right first-time approach.

5. Conclusions

Distortion prediction and compensation of a thin manifold structure, made of Inconel 718 and produced by LPBF, was investigated. The following conclusions were derived:

- The prediction of distortion was conducted in ANSYS Mechanical and ABAQUS using the inherent strain method. Both finite element codes showed very similar results in the prediction of distortion with a difference of less than 3% when comparing the peak predicted displacements. The predicted displacement distribution was also in agreement.
- Despite the overall positive distortion compensation results, the right first-time distortion compensation approach using predicted distortions proved to be challenging for the thin manifold structure as the distortions were overpredicted at the inner face of the component.
- For distortion compensation in LPBF, the accuracy in predicting the distortion in all areas of the geometry is key in order to deliver right first-time compensation for the thin manifold structure.
- The main barrier in the right first-time distortion compensation approach could be the lack of confidence in the predicted distortions. Therefore, further developments of the distortion predictive models for LPBF are required to gain more confidence in the accuracy without the need to print a physical part.
- The further developments can include detailed investigations on the geometrical limitations that the predictive models face. This will enable to understand which components and geometrical features can be compensated with the right first-time distortion compensation approach.

The following future work could be conducted in distortion compensation:

- The repeatability and reproducibility of distortion compensated parts need to be further tested in order to provide greater confidence in production.
- Improve the distortion compensation approaches where the predictive models for LPBF could be further enhanced as well as to be combined with machine learning and experimental approaches to deliver better solutions for distortion compensation.
- Investigation the feasibility of the data-driven and the right first-time distortion compensation approaches to other additive manufacturing processes (e.g. direct energy deposition, electron beam powder bed fusion and binder jetting) , where the data-driven distortion compensation can be directly applied while the right first-time approach would require the development of accurate physics-based predictive models for distortion.

Acknowledgment

Authors would like to thank 3T Additive Manufacturing LTD for supporting the 3D printing of the thin manifold component.

References

1. Wood, P.; Libura, T.; Kowalewski, Z. L.; Williams, G.; Serjouei, A. Influences of Horizontal and Vertical Build Orientations and Post-Fabrication Processes on the Fatigue Behavior of Stainless Steel 316L Produced by Selective Laser Melting. *Materials (Basel).* **2019**, *12* (24), 4203. https://doi.org/10.3390/ma12244203.

2. Xie, D.; Lv, F.; Liang, H.; Shen, L.; Tian, Z.; Zhao, J.; Song, Y.; Shuai, C. Towards a Comprehensive Understanding of Distortion in Additive Manufacturing Based on Assumption of Constraining Force. *Virtual Phys. Prototyp.* **2021**, 1–13. https://doi.org/10.1080/17452759.2021.1881873.

3. Parry, L.; Ashcroft, I. A.; Wildman, R. D. Understanding the Effect of Laser Scan Strategy on Residual Stress in Selective Laser Melting through Thermo-Mechanical Simulation. *Addit. Manuf.* **2016**, *12*, 1–15. https://doi.org/https://doi.org/10.1016/j.addma.2016.05.014.

4. Withers, P. J. Residual Stress and Its Role in Failure. *Reports Prog. Phys.* **2007**, *70* (12), 2211–2264. https://doi.org/10.1088/0034-4885/70/12/r04.

5. Marchese, G.; Atzeni, E.; Salmi, A.; Biamino, S. Microstructure and Residual Stress Evolution of Laser Powder Bed Fused Inconel 718 under Heat Treatments. *J. Mater. Eng. Perform.* **2021**, *30* (1), 565–574. https://doi.org/10.1007/s11665-020-05338-z.

6. Gruber, K.; Dziedzic, R.; Kuźnicka, B.; Madejski, B.; Malicki, M. Impact of High Temperature Stress Relieving on Final Properties of Inconel 718 Processed by Laser Powder Bed Fusion. *Mater. Sci. Eng. A* **2021**, *813*, 141111. https://doi.org/https://doi.org/10.1016/j.msea.2021.141111.

7. Chen, S.; Zhang, Y.; Wu, Q.; Gao, H.; Gao, Z.; Li, X. Effect of Solid-State Phase Transformation on Residual Stress of Selective Laser Melting Ti6Al4V. *Mater. Sci. Eng. A* **2021**, 141299. https://doi.org/https://doi.org/10.1016/j.msea.2021.141299.

8. Link, G.; Huntley, T.; Nickel, A.; Leitgeb, R.; Nguyen, T.; Prinz, F. B. Reducing Part Deformation by Inducing Phase Transformation. In *Solid Freeform Fabr. Symp.*; 1999; pp 727–734.

9. Parry, L. A.; Ashcroft, I. A.; Wildman, R. D. Geometrical Effects on Residual Stress in Selective Laser Melting. *Addit. Manuf.* **2019**, *25*, 166–175. https://doi.org/https://doi.org/10.1016/j.addma.2018.09.026.

10. Huo, Y.; Hong, C.; Li, H.; Liu, P. Influence of Different Processing Parameter on Distortion and Residual Stress of Inconel 718 Alloys Fabricated by Selective Laser Melting (SLM). *Mater. Res.* **2020**, *23* (6).

11. Bartlett, J. L.; Li, X. An Overview of Residual Stresses in Metal Powder Bed Fusion. *Addit. Manuf.* **2019**, *27*, 131–149. https://doi.org/https://doi.org/10.1016/j.addma.2019.02.020.

12. Mugwagwa, L.; Dimitrov, D.; Matope, S. A Methodology to Evaluate the Influence of Part Geometry on Residual Stresses in Selective Laser Melting. In *International*

Conference on Competitive Manufacturing; Stellenbosch, Stellenbosch University, South Africa, 2016.

13. Wan, H. Y.; Zhou, Z. J.; Li, C. P.; Chen, G. F.; Zhang, G. P. Effect of Scanning Strategy on Grain Structure and Crystallographic Texture of Inconel 718 Processed by Selective Laser Melting. *J. Mater. Sci. Technol.* **2018**, *34* (10), 1799–1804. https://doi.org/https://doi.org/10.1016/j.jmst.2018.02.002.

14. Pal, D.; Teng, C.; Stucker, B. Simulation of Powder-Based Additive Manufacturing Processes. In *Additive Manufacturing: Innovations, Advances, and Applications*; Srivatsan, T. S., Sudarshan, T. S., Eds.; CRC Press, 2015; p 199.

15. Peter, N.; Pitts, Z.; Thompson, S.; Saharan, A. Benchmarking Build Simulation Software for Laser Powder Bed Fusion of Metals. *Addit. Manuf.* **2020**, *36*, 101531. https://doi.org/https://doi.org/10.1016/j.addma.2020.101531.

16. Zeng, K.; Pal, D.; Gong, H. J.; Patil, N.; Stucker, B. Comparison of 3DSIM Thermal Modelling of Selective Laser Melting Using New Dynamic Meshing Method to ANSYS. *Mater. Sci. Technol.* **2015**, *31* (8), 945–956. https://doi.org/10.1179/1743284714Y.0000000703.

17. Michaleris, P. Modeling Metal Deposition in Heat Transfer Analyses of Additive Manufacturing Processes. *Finite Elem. Anal. Des.* **2014**, *86*, 51–60. https://doi.org/https://doi.org/10.1016/j.finel.2014.04.003.

18. Bangerth, W.; Hartmann, R.; Kanschat, G. Deal. II—a General-Purpose Object-Oriented Finite Element Library. *ACM Trans. Math. Softw.* **2007**, *33*, 24.

19. Wang, C.; Tan, X. P.; Tor, S. B.; Lim, C. S. Machine Learning in Additive Manufacturing: State-of-the-Art and Perspectives. *Addit. Manuf.* **2020**, *36*, 101538. https://doi.org/https://doi.org/10.1016/j.addma.2020.101538.

20. Chowdhury, S.; Mhapsekar, K.; Anand, S. Part Build Orientation Optimization and Neural Network-Based Geometry Compensation for Additive Manufacturing Process. *J. Manuf. Sci. Eng.* **2017**, *140* (3). https://doi.org/10.1115/1.4038293.

21. Francis, J.; Bian, L. Deep Learning for Distortion Prediction in Laser-Based Additive Manufacturing Using Big Data. *Manuf. Lett.* **2019**, *20*, 10–14. https://doi.org/https://doi.org/10.1016/j.mfglet.2019.02.001.

22. Pal, D.; Patil, N.; Zeng, K.; Stucker, B. An Integrated Approach to Additive Manufacturing Simulations Using Physics Based, Coupled Multiscale Process Modeling. *J. Manuf. Sci. Eng.* **2014**, *136* (6). https://doi.org/10.1115/1.4028580.

23. Pal, D.; Patil, N.; Kutty, K. H.; Zeng, K.; Moreland, A.; Hicks, A.; Beeler, D.; Stucker, B. A Generalized Feed-Forward Dynamic Adaptive Mesh Refinement and Derefinement Finite-Element Framework for Metal Laser Sintering—Part II: Nonlinear Thermal Simulations and Validations2. *J. Manuf. Sci. Eng.* **2016**, *138* (6). https://doi.org/10.1115/1.4032078.

24. Mukherjee, T.; Zhang, W.; DebRoy, T. An Improved Prediction of Residual Stresses and Distortion in Additive Manufacturing. *Comput. Mater. Sci.* **2017**, *126*, 360–372. https://doi.org/https://doi.org/10.1016/j.commatsci.2016.10.003.

25. Mukherjee, T.; Manvatkar, V.; De, A.; DebRoy, T. Mitigation of Thermal Distortion during Additive Manufacturing. *Scr. Mater.* **2017**, *127*, 79–83.

https://doi.org/https://doi.org/10.1016/j.scriptamat.2016.09.001.

26. Williams, R. J.; Davies, C. M.; Hooper, P. A. A Pragmatic Part Scale Model for Residual Stress and Distortion Prediction in Powder Bed Fusion. *Addit. Manuf.* **2018**, *22*, 416–425. https://doi.org/https://doi.org/10.1016/j.addma.2018.05.038.

27. Denlinger, E. R.; Heigel, J. C.; Michaleris, P. Residual Stress and Distortion Modeling of Electron Beam Direct Manufacturing Ti-6Al-4V. *Proc. Inst. Mech. Eng. Part B J. Eng. Manuf.* **2014**, *229* (10), 1803–1813. https://doi.org/10.1177/0954405414539494.

28. Biegler, M.; Elsner, B. A. M.; Graf, B.; Rethmeier, M. Geometric Distortion-Compensation via Transient Numerical Simulation for Directed Energy Deposition Additive Manufacturing. *Sci. Technol. Weld. Join.* **2020**, 1–8. https://doi.org/10.1080/13621718.2020.1743927.

29. Afazov, S.; Denmark, W. A. D.; Lazaro Toralles, B.; Holloway, A.; Yaghi, A. Distortion Prediction and Compensation in Selective Laser Melting. Addit. Manuf. 2017, 17, 15–22.

30. Murakawa, H.; Luo, Y.; Ueda, Y. Prediction of Welding Deformation and Residual Stress by Elastic FEM Based on Inherent Strain. *J. Soc. Nav. Archit. Japan* **1996**, *1996* (180), 739–751. https://doi.org/10.2534/jjasnaoe1968.1996.180_739.

31. Huang, H.; Ma, N.; Chen, J.; Feng, Z.; Murakawa, H. Toward Large-Scale Simulation of Residual Stress and Distortion in Wire and Arc Additive Manufacturing. *Addit. Manuf.* **2020**, *34*, 101248. https://doi.org/https://doi.org/10.1016/j.addma.2020.101248.

32. Chen, Q.; Liang, X.; Hayduke, D.; Liu, J.; Cheng, L.; Oskin, J.; Whitmore, R.; To, A. C. An Inherent Strain Based Multiscale Modeling Framework for Simulating Part-Scale Residual Deformation for Direct Metal Laser Sintering. *Addit. Manuf.* **2019**, *28*, 406–418. https://doi.org/https://doi.org/10.1016/j.addma.2019.05.021.

33. Afazov, S.; Frame, J.; Ankalkhope, U.; Bidare, P.; Liu, Y.; Vesga, W.; Dutton, B. Prediction of Residual Stress Evolution for End-to-End Process Chain of Laser Powder Bed Fusion Process and Determination of Fatigue S-N Curves. In *ASTM STP 1631 On Structural Integrity of Additive Manufactured Materials and Parts*; 2020.

34. O'Brien, J. M.; Montgomery, S.; Yaghi, A.; Afazov, S. M. Process Chain Simulation of Laser Powder Bed Fusion Including Heat Treatment and Surface Hardening. *CIRP J. Manuf. Sci. Technol.* **2021**, *32*, 266–276. https://doi.org/https://doi.org/10.1016/j.cirpj.2021.01.006.

35. Yaghi, A.; Ayvar-Soberanis, S.; Moturu, S.; Bilkhu, R.; Afazov, S. Design against Distortion for Additive Manufacturing. *Addit. Manuf.* **2019**, *27*, 224–235. https://doi.org/https://doi.org/10.1016/j.addma.2019.03.010.

36. Afazov, S.; Okioga, A.; Holloway, A.; Denmark, W.; Triantaphyllou, A.; Smith, S.-A.; Bradley-Smith, L. A Methodology for Precision Additive Manufacturing through Compensation. *Precis. Eng.* **2017**, *50*, 269–274. https://doi.org/https://doi.org/10.1016/j.precisioneng.2017.05.014.

37. Afazov, S.; Semerdzhieva, E.; Scrimieri, D.; Serjouei, A.; Kairoshev, B.; Derguti, F. An Improved Distortion Compensation Approach for Additive Manufacturing Using Optically Scanned Data. *Virtual Phys. Prototyp.* **2021**, *16* (1), 1–13. https://doi.org/10.1080/17452759.2021.1881702.

38. Yang, T.; Xie, D.; Yue, W.; Wang, S.; Rong, P.; Shen, L.; Zhao, J.; Wang, C. Distortion of Thin-Walled Structure Fabricated by Selective Laser Melting Based on Assumption of Constraining Force-Induced Distortion. *Metals (Basel).* **2019**, *9* (12), 1281. https://doi.org/10.3390/met9121281.

39. Megahed, M.; Mindt, H.-W.; N'Dri, N.; Duan, H.; Desmaison, O. Metal Additive-Manufacturing Process and Residual Stress Modeling. *Integr. Mater. Manuf. Innov.* **2016**, *5* (1), 61–93. https://doi.org/10.1186/s40192-016-0047-2.

40. Ding, J.; Colegrove, P.; Mehnen, J.; Ganguly, S.; Sequeira Almeida, P. M.; Wang, F.; Williams, S. Thermo-Mechanical Analysis of Wire and Arc Additive Layer Manufacturing Process on Large Multi-Layer Parts. *Comput. Mater. Sci.* **2011**, *50* (12), 3315–3322. https://doi.org/https://doi.org/10.1016/j.commatsci.2011.06.023.

41. Papadakis, L.; Loizou, A.; Risse, J.; Bremen, S.; Schrage, J. A Computational Reduction Model for Appraising Structural Effects in Selective Laser Melting Manufacturing. *Virtual Phys. Prototyp.* **2014**, *9* (1), 17–25. https://doi.org/10.1080/17452759.2013.868005.

42. Neugebauer, F.; Keller, N.; Ploshikhin, V.; Feuerhahn, F.; Koehler, H. *Multi Scale FEM Simulation for Distortion Calculation in Additive Manufacturing of Hardening Stainless Steel*; 2014.

43. Roberts, I. A.; Wang, C. J.; Esterlein, R.; Stanford, M.; Mynors, D. J. A Three-Dimensional Finite Element Analysis of the Temperature Field during Laser Melting of Metal Powders in Additive Layer Manufacturing. *Int. J. Mach. Tools Manuf.* **2009**, *49* (12), 916–923. https://doi.org/https://doi.org/10.1016/j.ijmachtools.2009.07.004.

44. Hill, R. *The Mathematical Theory of Plasticity*; Oxford University Press: New York, 1983.

45. EOS GmbH—Electro Optical Systems, Material EOS Nickel Alloy IN718 Data Sheet for EOS DMLS EOSINT M280 400W & M290 400W systems, Munich, Germany https://ip-saas-eos-cms.s3.amazonaws.com/public/4528b4a1bf688496/ff974161c2057e6df56db5b67f0f5595/EOS_NickelAlloy_IN718_en.pdf (accessed February 10, 2021).

46. Afazov, S. M.; Becker, A. A.; Hyde, T. H. Development of a Finite Element Data Exchange System for Chain Simulation of Manufacturing Processes. *Adv. Eng. Softw.* **2012**, *47* (1), 104–113. https://doi.org/https://doi.org/10.1016/j.advengsoft.2011.12.011.